Chemical Physics Letters 842 (2024) 141197

Contents lists available at ScienceDirect

Chemical Physics Letters

journal homepage: www.elsevier.com/locate/cplett

The binding of auranofin at DNA/RNA nucleobases: A DFT assessment

Iogann Tolbatov [a], Paolo Umari [a], Tiziano Marzo [b], Lorenzo Chiaverini [b], Diego La Mendola [b], Alessandro Marrone [c,*]

[a] Department of Physics and Astronomy, University of Padova, via F. Marzolo 8, 35131 Padova, Italy
[b] Department of Pharmacy, University of Pisa, Via Bonanno Pisano 6, 56126 Pisa, Italy
[c] Dipartimento di Farmacia, Università degli Studi "G. D'Annunzio" Chieti-Pescara, Via dei Vestini 31, 66100 Chieti, Italy

ARTICLE INFO

Keywords:
Density functional theory
Auranofin
DNA and RNA nucleobases
Dissociation enthalpy and free energy
Calculated UV–vis spectra

ABSTRACT

A variety of therapies are based on cytotoxicity induced via hampering the DNA and/or RNA homeostasis. The metallodrugs' forerunner, cisplatin, is exemplificative of the tremendous biological effects of nucleobase targeting, and a large body of researches to discover novel metallodrugs. In this paper, DFT approaches were employed to investigate the structure, stability and electronic properties of the complexes formed by the $[Et_3PAu]^+$ metal fragment generated by auranofin -or its derivatives- and the DNA/RNA nucleobases. Therefore, TDDFT calculations were performed to assess the viability of the spectrophotometric quantification of the $[Et_3PAu]^+$-nucleobase adducts.

1. Introduction

The blockage or hampering of nucleic acids' functions is a potent and cross-genera strategy to induce cytotoxicity and is widely adopted for pharmacological purposes. However, while most cytotoxic agents have been recognized to target DNA or protein [1–3], RNA-specific drugs are much less common [4,5].

The DNA and RNA nucleobases are characterized by a widespread reactivity, and several ways to alter the bioinformation they deliver are viable [6,7]. Amazingly, the chemical modification of nucleobases could be operated either *in vivo*, when the reactive agent is administered and its reaction with DNA or RNA nucleobases occurs in the cell, or *in vitro* by producing a modified nucleobase that is subsequently delivered [8]. Thus, several nucleoside mimicking drugs have been developed for anticancer, antibacterial, and antiviral therapy [9–12].

Among the many agents able to react with nucleotides, metal compounds have attracted a notable attention since the discovery of the anticancer activity of the prodrug *cis*-dichloro-diamino-platin, i.e. cisplatin [13]. The high affinity of its $[Pt(NH_3)_2]^{2+}$ active metal fragment for the purine nucleobases of DNA duplexes, is distinctive of the cisplatin mechanism of action [14]. The widespread exploration of the chemical space around this Pt(II) complex, in the attempt to identify more potent and less toxic analogues, has been an invaluable stimulus to the development of the "metals in medicine" discipline [15].

Concomitantly, other metal agents employed in therapy have been tested to evaluate their potential binding at DNA, and their possible repurposing in the anticancer therapy [16]. Gold(III) [17,18] and, mostly, gold(I) [19–21] complexes have been long recognized as therapeutically active compounds. The well-known anti-arthritic complex auranofin, (1-Thio-β-D-glucopyranosatotriethylphosphine gold-2,3,4,6-tetraacetate, AF), as well as its halide derivatives (Fig. 1a), have been recently considered in repurposing studies of its anticancer, antibacterial, antiviral and antiparasitic potential [20,22–25]. On the other hand, the possible targeting of RNA or DNA polynucleotides by gold(I) scaffolds remains largely unexplored [26].

AF has been found to cause oxidative DNA damages in cancer cells [27] by raising the level of ROS well beyond their antioxidant and self-repairing abilities [28]. An impact of AF on the viral DNA dynamics through an antiproliferative effect has been also suggested [29]. Recently, it has been shown that while AF itself does not react with DNA [30], its halide analogues, Et_3PAuCl and Et_3PAuI, can bind at and rigidify DNA duplexes [25].

The studies of the AF-RNA interaction are much scarcer. Recently, AF was found to decrease the amount of mRNA coding the interleukin IL-1β and tumor necrosis factor TNF-α [31]. The induction of pro-IL-1β and the inflammasome receptor NLRP3 has been shown to be suppressed by AF [32]. Therefore, the inhibition of several pro-inflammatory signaling pathways mediated by cytokines has been ascribed to auranofin [33].

In this study, the binding at nucleobases of the $[Et_3PAu]^+$ metal fragment -generated by auranofin or its analogues (Fig. 1)-, and its

* Corresponding author.
E-mail address: amarrone@unich.it (A. Marrone).

https://doi.org/10.1016/j.cplett.2024.141197
Received 30 January 2024; Received in revised form 6 March 2024; Accepted 8 March 2024
Available online 11 March 2024

structural impact on the stability of polynucleotide structures was investigated by using density functional theory approach. The binding of the active gold(I) metal fragment $[Et_3PAu]^+$ on pyridyl nitrogens of A, G, C, T, and U was found to only slightly modify the electronic structure of each nucleobase and marginally affect their complementarity. On the other hand, atomic charges and both shape and energy of frontier molecular orbitals were found to be modulated by leading to a different UV–Vis absorption profile. The here reported computational results represent a valuable basis of information for future experimental and/or theoretical investigations specifically addressed to either AF-DNA or AF-RNA binding, as well as the coordination of the $[Et_3PAu]^+$ metal fragment at nucleotide cofactors, such as NAD, AMP, GMP. Hypotheses on the potential implications in the development of therapeutic applications of the AF-nucleobase binding are eventually drawn and discussed.

2. Materials and methods

The Gaussian 16 quantum chemistry package was employed for all computations [34]. DFT allows for accurate characterization of transition metal complexes with biomolecules [35], including coinage metals [36–38]. All structures were optimized in water with the hybrid range-corrected functional ωB97X-D [39] and the def2SVP basis set [40,41]. Such a computational approach had been found to yield reliable geometrical structures and precise estimations of the electronic and solvation energies of other metal–biomolecule adducts [42–44]. Frequency computations verified the stationary nature of the minima and produced the zero-point energy (ZPE) and vibrational corrections to the thermodynamic properties. The harmonic approximation was adopted to compute the zero-point energy, thermal, and entropy corrections and yield the Gibbs free energy of each investigated system. The IEFPCM formalism was employed to account for the solvation free energy in water [45].

The calculation of the UV–Vis spectra was done on the structures preoptimized with the hybrid functional B3LYP [46,47] and basis set def2TZVP [40,41] in water with the ultrafine grid for numerical integrations and the fine grid for solving the CPHF equations. The TDDFT calculations were done with the same parameters, solving for 12 states, taking into account only singlet excited states.

The NBO analysis [48], performed in water at the level ωB97X-D/def2SVP, allowed the assessment of the strength of the hydrogen bond interactions in either free or metalated nucleobase pairs.

3. Results and discussion

The binding of the auranofin fragment $[Et_3PAu]^+$ at the pyridyl nitrogen atoms of both DNA and RNA nucleobases was investigated by using density functional theory. The assumed nucleic targets of $[Et_3PAu]^+$ included the native forms of A, C, and G, whereas both T and U were assumed into two non-native protomeric forms, a and b, featured by a pyridyl site on the N_1 atom (Fig. 2). Notably, by taking into account all the pyridyl sites available on the nucleobase scaffolds, independently on their involvement in the complementary hydrogen bonds duplex DNA or RNA, we aimed at probing the coordination of the $[Et_3PAu]^+$ metal fragment to either single stranded DNA or RNA fragments, as well as the nucleobase scaffold of cellular nucleotide cofactors such as NAD, AMP, and GMP.

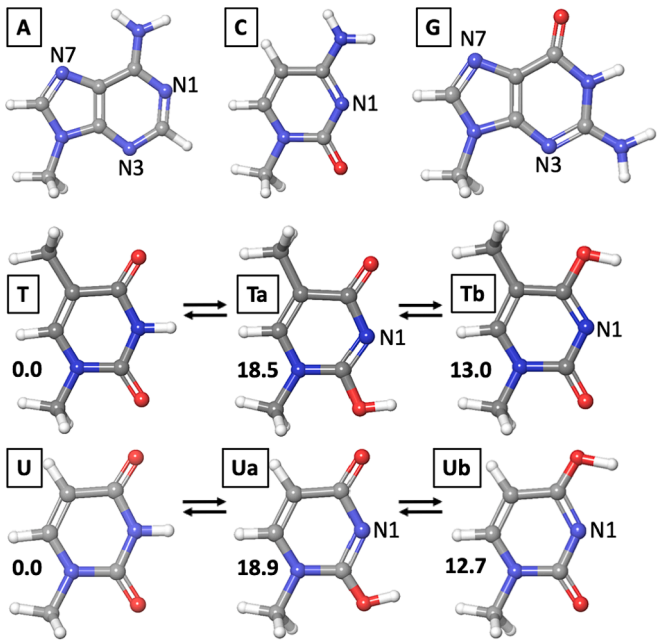

Fig. 2. The nucleobase structures potentially targeted by AF. The pyridyl nitrogen atoms, assumed as the metal binding sites on A, G, and C nucleobases and the Ta/b and Ua/b tautomers of T and U, respectively, are indicated. GFE energies for tautomers of T and U are indicated in kcal/mol.

All adducts between $[Et_3PAu]^+$ and the selected nucleobase scaffolds were optimized at DFT level of theory as described in the Materials and Methods section.

As expected, the binding of the auranofin fragment led to only slight modifications of the nucleobase scaffolds with bond and angle deviations of ≤ 0.01 Å and ≤ 2 degrees, respectively (Table S1). Therefore, the calculated geometrical parameters describing the coordination of the $[Et_3PAu]^+$ fragment at nucleobase scaffolds were found in good agreement with the available literature data (Table S2), thus corroborating the reliability of the employed DFT approach.

The strength of the Au–N coordinative bond in the examined complexes was investigated by the calculation of the corresponding dissociation enthalpy (BDE) and free energy (BDFE). In this case, we assumed to take apart and relax the auranofin and nucleobase fragments of each complex, and to estimate the energy cost for this process occurring in water. As expected, the BDFE values were on overall lower than BDE values, because of the translational entropy increase in the dissociation process (Table 1).

Both energy parameters were found in rather narrow ranges, i.e. 34–41 and 21–28 kcal/mol for BDE and BDFE, respectively, which indicates quite similar strengths of the Au–N coordinative bonds. On the other hand, both U and T complexes can be formed only if the nucleobase bears either the a or b protomeric form (Fig. 2), thus requiring extra energy costs (Table 1). As a consequence, the relaxation of the U or T fragment to the corresponding naïve forms reduced the BDE and BDFE by 13–18 kcal/mol, thus indicating a weaker coordination of the AF

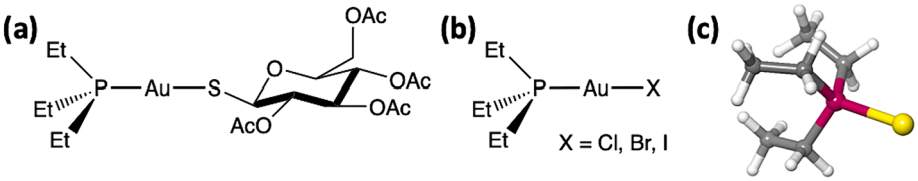

Fig. 1. Chemical structure of Auranofin (a), its halide derivatives (b), and its pharmacophore part $[Et_3PAu]^+$ (c). Color scheme used here and below: Au (yellow), P (burgundy), O (red), N (blue), C (grey), H (white).

Table 1
The bond dissociation enthalpy (BDE) and bond dissociation free energy (BDFE) values for the metalated bases in kcal/mol. In case of T and U, the BDE and BDFE values including the relaxation to the naïve form with protonated nitrogen are indicated in parentheses.

Metalated base	BDE	BDFE
$[Et_3PAu(A^1)]^+$	36.2	26.5
$[Et_3PAu(A^3)]^+$	36.3	25.5
$[Et_3PAu(A^7)]^+$	37.4	27.0
$[Et_3PAu(C^1)]^+$	39.7	27.9
$[Et_3PAu(G^3)]^+$	33.7	21.1
$[Et_3PAu(G^7)]^+$	41.2	28.3
$[Et_3PAu(Ta^1)]^+$	36.9 (18.5)	25.9 (7.4)
$[Et_3PAu(Tb^1)]^+$	35.8 (23.0)	24.5 (11.5)
$[Et_3PAu(Ua^1)]^+$	36.4 (17.5)	25.3 (6.4)
$[Et_3PAu(Ub^1)]^+$	36.2 (23.9)	22.9 (10.3)

fragment at these nucleobases. Interestingly, the stronger Au–N coordination was detected in the $[Et_3PAu(G^7)]^+$ complex, resembling the well-known cisplatin preference for this nucleobase site [14]. On the other hand, both C1 and A7 complexes presented BDE and BDFE values only 1.5 kcal/mol lower compared to the G7 complex, thus, all these sites must be assigned approximately the same affinity for the $[Et_3PAu]^+$ fragment.

The appreciably stronger binding of AF to purines, A and G, and to C, compared to U and T led us to state that AF did not presumably present any chemoselectivity for either DNA or RNA. On the other hand, DNA and RNA nucleobases are characterized by different chemical environment that could significantly modulate their metallophilicities. For example, while DNA mostly holds the double helix and the nucleobase pairs' stacking structure, RNA presents a wider variety of structural motives, including monostrand segments. In this frame, for example, the binding at C^1 in the DNA structure is expected to be hampered by the involvement of the N1 site in the GC complementarity, while the binding of C^1 on monostrand motives of RNA might still occur. Analogously, while the N_3 and N_7 of adenine and guanine are the only coordinative site available in duplex structures, the N_1 atom can be targeted by $[Et_3PAu]^+$ in either single stranded DNA/RNA or cellular nucleotide cofactors.

The calculated BDE and BDFE values relative to $[Et_3PAu]^+$-nucleobase complexes clearly indicated that the AF fragment is able to form highly stable complexes with either DNA or RNA, by binding to the nucleobases with available pyridyl nitrogen atoms on their naïve forms, i.e. A, G and C.

To better assess the response of DNA or RNA duplex structure to the binding of AF, the stability of the complementary nucleobase pairs of A, G and C, i.e. AT/AU and GC, in their either metalated or free form was computationally assayed. The detachment enthalpy (DE) and detachment free energy (DFE) values for taking apart the two nucleobase fragments were calculated and reported in Table 2. On overall, metalation alter slightly the stability of the nucleobase complementarity. The DE or DFE values for each free or metalated base pair ranged within 1–2 kcal/mol (Table 2), thus, close to the computational accuracy limit expected for these estimates. On the other hand, it is worth noticing the different response to the metalation disclosed by AT/AU and GC pairs. The nucleobase pairs formed by A were characterized by DFE decreasing upon metalation, whereas the GC pair was characterized by DFE increasing (Table 2). Despite its low entity, such an AF-induced modulation of the base pair complementarity may affect some of the DNA or RNA functionalities, for instance, when mechanisms of controlled unfolding and unpairing of the duplex structures must be operated.

Table 2
The DE and DFE values for the naïve and metalated base pairs in kcal/mol.

base pair	DE	DFE
AT	13.9	4.3
$[Et_3PAu(A^3T)]^+$	14.1	2.5
$[Et_3PAu(A^7T)]^+$	14.5	4.2
AU	13.9	4.0
$[Et_3PAu(A^3U)]^+$	14.1	2.1
$[Et_3PAu(A^7U)]^+$	14.4	3.5
GC	21.8	9.7
$[Et_3PAu(G^3C)]^+$	25.1	10.5
$[Et_3PAu(G^7C)]^+$	22.3	11.5

Therefore, the binding of the cationic Au(I) fragment is expected to affect the electron distribution within the bonded nucleobase or nucleobase pairs. In fact, our calculations revealed that the metalation of single nucleobases led to a very small decrease of the HOMO-LUMO (HL) gap compared to the relative free nucleobase, thus evidencing that the coordination of the $[Et_3PAu]^+$ fragment did not appreciably change the electronic structure and, in turn, the reactivity of the nucleobases (Tables 3 and 4).

However, it is worth noticing that the variation of the HL gap for the GC base pair was calculated to be about 0.4 eV, appreciably larger compared to either AT or AU. A deeper analysis of the frontier molecular orbitals was thus performed through the visualization and comparison of the isodensity surfaces for the orbitals within the HOMO-5 and LUMO + 5 range for the GC and AU base pairs. The HOMO of both GC and AU base pairs (in their naïve form) bear a π character and are localized on the purine fragment (Fig. 3). The binding of the $[Et_3PAu]^+$ fragment at the N_7 of either G or A caused, as expected, an appreciable HOMO stabilization of –0.48 and –0.64 eV in the GC and AU metal complexes, respectively. Intriguingly, while the $[Et_3PAuG^7C]^+$ complex was featured by a purine-localized HOMO resembling the HOMO of the naïve GC pair (Fig. 3), the HOMO of the $[Et_3PAuA^7U]^+$ adduct was pyrimidine-localized and featured by an orbital energy that is about 0.17 eV higher than the purine-localized HOMO-1 (Fig. 3). Hence, the larger HL gap variation detected for the GC compared to the AU base pair is ascribable to the more pronounced stabilization of the π purine-localized orbital that, in the metalated AU but not in the metalated GC system, is shifted below the π pyrimidine-localized orbital (Fig. 3).

The response to the Au(I) moiety binding disclosed by the virtual frontier orbitals also reflected their localization. Both GC and AU naïve base pairs are featured by two virtual π orbitals, lying at low energy, one localized on the purine base – the lowest energy lying in both cases –, and one localized on the pyrimidine base. The binding of the cationic metal fragment, as expected, was found to induce a more pronounced stabilization of the purine-localized virtual orbitals in both GC and AU adducts (Fig. 3). It is also worth noticing how the either occupied or virtual pyrimidine-localized π orbitals resulted instead destabilized by the binding of the $[Et_3PAu]^+$ fragment. These data is likely ascribable to the charge redistribution occurring in force of the positive charge delivered by the metal fragment, and causing a slight increase of the electronic charge on the pyrimidine moiety.

Thus, the binding of the metallic cationic fragment was found to be able to globally affect the charge distribution in nucleobase pairs even though, as an effect of compensation, the nucleobase complementarity is only negligibly affected, as already inferred by DE and DFE data. Indeed, while the binding of $[Et_3PAu]^+$ at A or G in their respective complementary base pairs led to an increase of the positive charge on the metalated nucleobase, the overall strength of the interbase hydrogen

Table 3
HL gap (in eV) for the naïve and metalated nucleobases on the position 7 (A and G) or 1(C, T and U). The HP gap values assigned to the U and T tautomers are labelled by the a and b exponents.

nucleobase	HL gap	
	naïve	metalated
A	9.285	9.151
C	9.481	9.210
G	9.381	9.074
T	9.363	9.504^a, 8.898^b
U	9.559	9.634^a, 9.163^b

Table 4
HL gap (in eV) for the naïve and metalated (on the position 7 of the involved purine) nucleobase pairs AT, AU, and GC.

nucleobase pair	HL gap naïve	metalated
AT	9.073	8.995
AU	8.977	9.132
GC	8.421	8.825

bonds remained almost unaffected (Table 2).

The second order NBO analysis allowed us to quantify the strength of the hydrogen bond interactions in either free or metalated nucleobase pairs, and to evidence their metal-induced modulation (Fig. 4). On overall, we found a weakening of the hydrogen bonds involving the metalated nucleobase as HB acceptor, and a strengthening of the hydrogen bonds involving the metalated nucleobase as HB donor. This outcome is consistent with the increase of the positive charge in the metalated nucleobase that is expected to exalt the HB donor character and fade the HB acceptor character. Intriguingly, while the AT and AU pairs present two hydrogen bonds, in which the metalated A is either donor or acceptor, the GC pair presents three hydrogen bonds, two of which see the guanine involved as the HB donor. This outcome explains in detail the overall stabilizing effect of the metalation in GC compared to the overall destabilizing effect on the AT or AU pairs, and provides for a better understanding of the low structural impact of the AF binding at nucleic biotargets (Table 5).

The low structural impact of AF coordination to either DNA or RNA, emerging from our DFT calculations, highlights the importance of the quantification of the amount of $[Et_3PAu]^+$ bound per DNA or RNA fragment. Indeed, we envision that only a large amount of AF-bound units might be able to hamper or alter the functionality of DNA or RNA. In this frame, TD-DFT calculations were performed with the aim of paving the basis for the development of spectrophotometric methods for the qualification and quantification of the binding of the $[Et_3PAu]^+$ moiety at DNA or RNA. The calculated UV–vis spectra of non-activated auranofin (AF), its derivative pharmacophore $[Et_3PAu]^+$, single nucleobases A and G as well as their metalated forms are shown in Figs. 5, 6, S1, and S2. The selection of the nucleobases for the TDFFT study is based on the relatively strong bonds with Au of A and G. As shown, the free nucleobase systems are characterized by quite similar profiles of absorbance bands, in the region 175–275 nm (Fig. 5), which seemingly preclude a spectrophotometric qualification of metalation, whereas the metalated nucleobases shift the profile to the right, i.e. to the range 200–300 nm (Figs. 5 and 6). For instance, the calculated UV–vis spectra of the metalated A^7 presents a wide band around 250 nm dominated by the HOMO→LUMO transition at 257.1 nm; in fact the metalated G^7 also displays a wide band around 250 nm even though emerging from two transitions, i.e. HOMO→LUMO+1 and HOMO→LUMO at 242.3 and 267.4 nm, respectively. Such an example shows that the spectrophotometric differentiation of the A or G metalation is probably unfeasible.

On the other hand, in all examined nucleobase complexes, we found that metalation led to spectra with no absorbance in the region around 325 nm. This latter outcome indicated that the metalation process could be spectroscopically followed up by the disappearance of the HOMO→LUMO band at 325.7 nm in the spectra of the unbound $[Et_3PAu]^+$ moiety (Fig. S1), with the caveat that such a metal-related band is detectable in the examined experimental conditions. On this basis, we envision that UV–vis spectrophotometric methods can be calibrated to quantify the fraction of $[Et_3PAu]^+$ moieties bound at DNA or RNA fragments or coordinated by cellular nucleotide cofactors, especially when in vitro experiments or assays are concerned.

Moreover, the band at 325.7 nm, which we found diagnostic of the free $[Et_3PAu]^+$ complex, may serve as the indicator of activation of AF, since the spectrum of AF is limited by the HOMO→LUMO band at 272.0 nm to the right (Fig. S1), the value corresponding well to the experimental value of 280 nm [49].

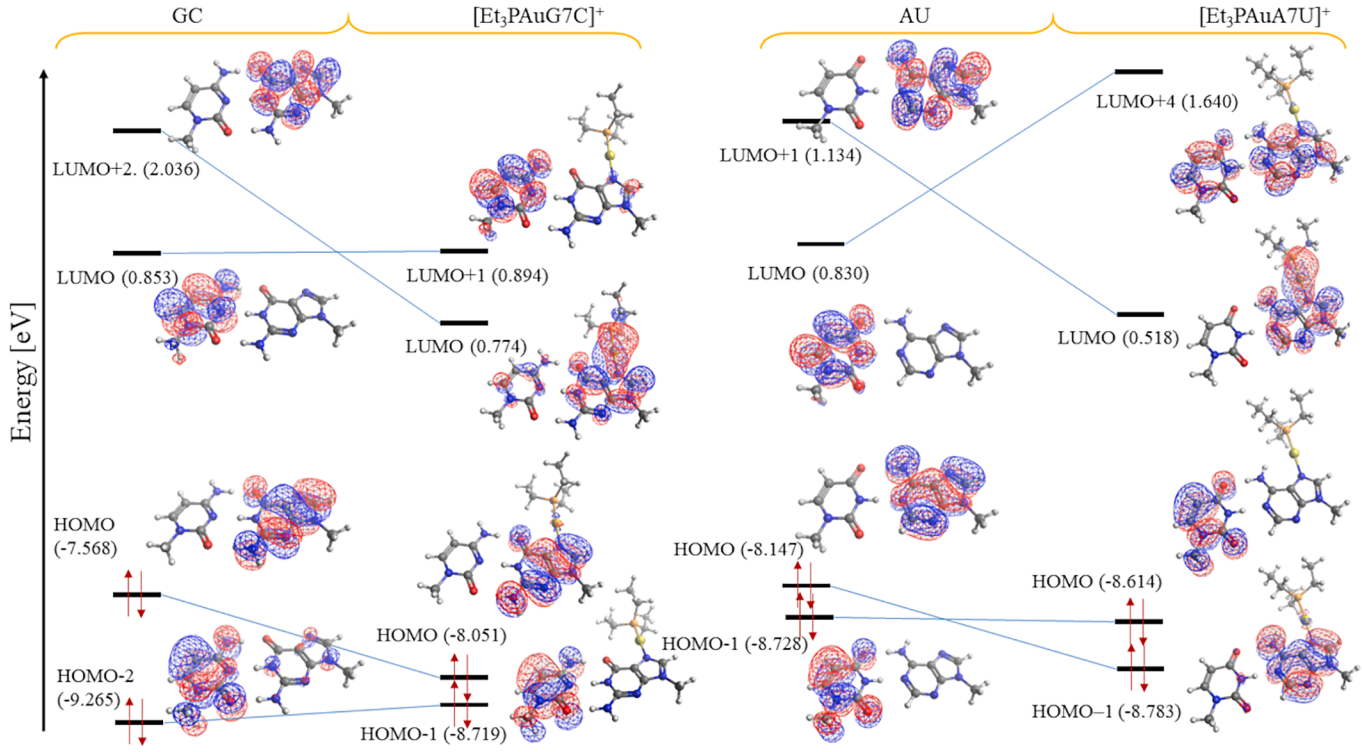

Fig. 3. Energy diagrams of the frontier π orbitals for naïve and metalated GC (left) and AU (right) base pairs. The stabilization or destabilization of the molecular orbitals due to the binding of the $[Et_3PAu]^+$ fragment at the N_7 on the purine fragment is represented with blue connector lines. A rendition of the isodensity surfaces for the sketched molecular orbitals is also provided (blue and red colors depict the sign of the represented orbital).

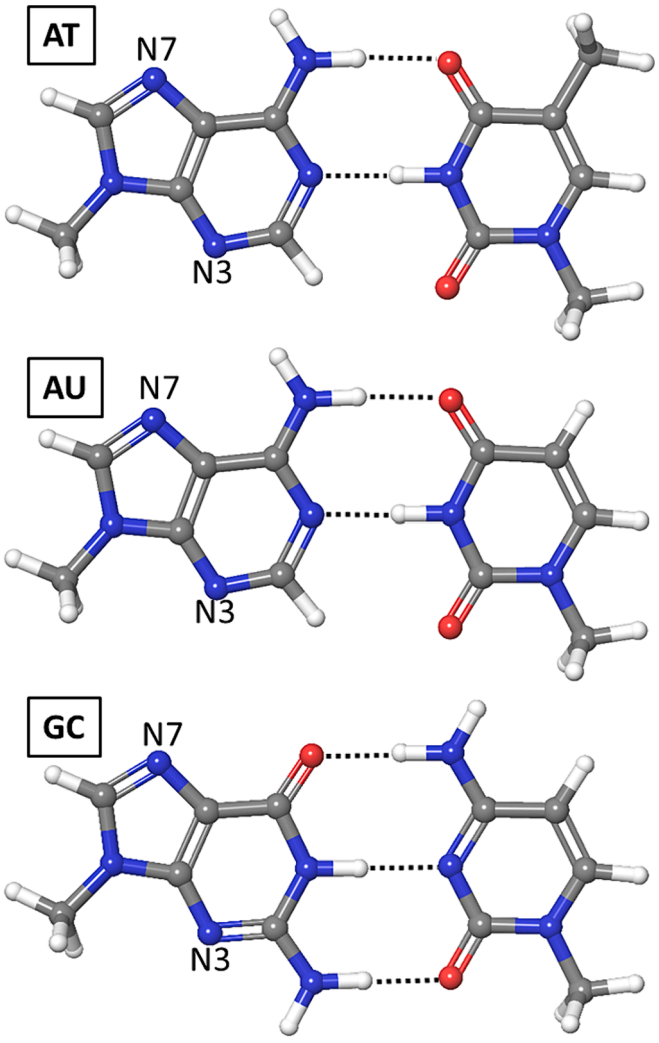

Fig. 4. Studied base pairs with indicated metal binding sites. Interbase hydrogen bonds (distance between connected non-hydrogen atoms < 2.0 Å) are indicated by dashed lines.

Table 5
NBO charge distribution (m = metal fragment), interbase H-bond lengths (in Angstrom) for the naïve and metalated base pairs, and estimates of H-bond strength (in kcal/mol) via second order perturbation analysis (SOP) provided by NBO calculations. The donating→accepting nucleobases are indicated.

nucleobase pair	NBO charge	H-bonds length	SOP
AT	A(0.027) + T(-0.027)	1.88 $^{A\rightarrow T}$, 1.77 $^{T\rightarrow A}$	19.5, 37.0
[Et_3PAu (A^3T)]$^+$	m(0.792) + A(0.221) + T(-0.013)	1.85 $^{A\rightarrow T}$, 1.79 $^{T\rightarrow A}$	21.7, 33.0
[Et_3PAu (A^7T)]$^+$	m(0.793) + A(0.222) + T(-0.015)	1.84 $^{A\rightarrow T}$, 1.79 $^{T\rightarrow A}$	22.2, 34.0
AU	A(0.028) + U(-0.028)	1.88 $^{A\rightarrow U}$, 1.77 $^{U\rightarrow A}$	19.5, 37.25
[Et_3PAu (A^3U)]$^+$	m(0.792) + A(0.222) + U(-0.014)	1.85 $^{A\rightarrow U}$, 1.79 $^{U\rightarrow A}$	21.6, 33.3
[Et_3PAu (A^7U)]$^+$	m(0.793) + A(0.223) + U(-0.016)	1.85 $^{A\rightarrow U}$, 1.79 $^{U\rightarrow A}$	21.85, 34.5
GC	G(-0.061) + C(0.061)	1.81 $^{C\rightarrow G}$, 1.86 $^{G\rightarrow C}$, 1.78 $^{G\rightarrow C}$	24.95, 29.3, 26.1
[Et_3PAu (G^3C)]$^+$	m(0.780) + G(0.132) + C(0.088)	1.82 $^{C\rightarrow G}$, 1.83 $^{G\rightarrow C}$, 1.71 $^{G\rightarrow C}$	23.2, 33.1, 33.75
[Et_3PAu (G^7C)]$^+$	m(0.766) + G(0.159) + C(0.075)	1.82 $^{C\rightarrow G}$, 1.83 $^{G\rightarrow C}$, 1.76 $^{G\rightarrow C}$	22.15, 32.0, 28.1

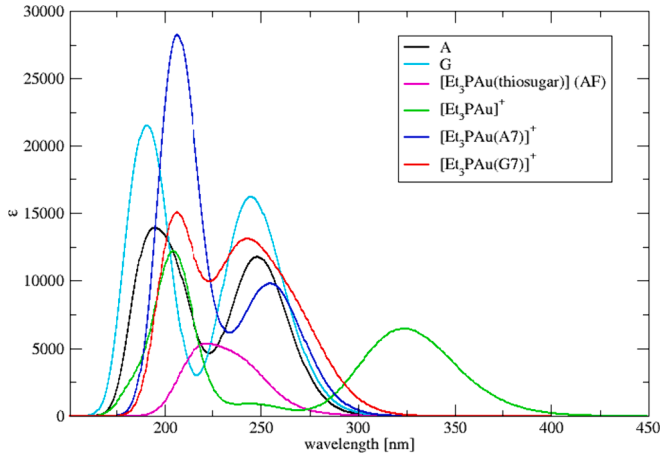

Fig. 5. Comparison of the calculated UV–vis spectra for $[Et_3PAu]^+$, A, G, $[Et_3PAu(A^7)]^+$ and $[Et_3PAu(G^7)]^+$.

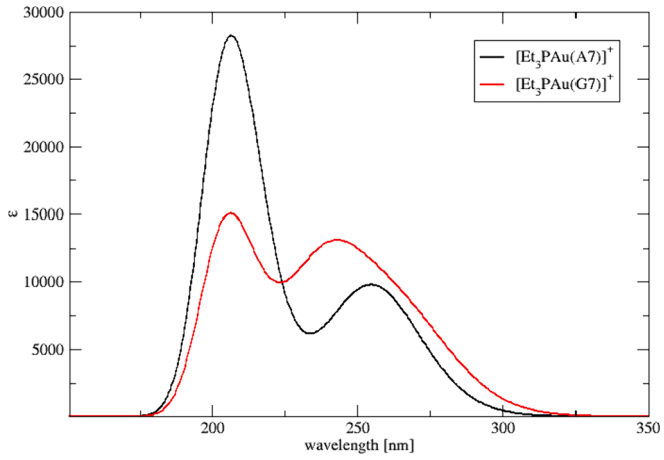

Fig. 6. Comparison of the calculated spectra for $[Et_3PAu(A^7)]^+$ and $[Et_3PAu(G^7)]^+$.

4. Conclusions

To resume, along the intensive efforts devoted to the repurposing of AF and its halide-based analogues, the present computational investigation aimed at assessing the possible targeting of either DNA or RNA. Indeed, while the main targets for gold(I) drugs activity are reputed to be some protein systems; the interactions with nucleic acids is still a largely unexplored hypothesis, though the potential impact on the overall pharmacological profile of AF and gold-based therapeutics [50]. We focused on the binding of the active scaffold $[Et_3PAu]^+$ at the nucleosides A, C, G, T, and U on the structural effects of this nucleobase metalation. We found that the coordination of the gold(I) pharmacophore $[Et_3PAu]^+$ on pyridyl nitrogens of A, G, C, T, and U only marginally altered the electronic structure of each nucleobase and thus slightly changed their complementarity. Intriguingly, we detected a weakening of the hydrogen bonds incorporating the metalated nucleobase as acceptor and a reinforcement of the hydrogen bonds involving the metalated nucleobase as donor, ascribable to the increased positive charge in the metalated nucleobase.

Also, the UV–vis spectra for the $[Et_3PAu]^+$-bound and unbound nucleobases A and G, comparatively more favorable toward metalation, were calculated by TDDFT approaches. We evidenced that, while the metalation results in a slight ~ 25 nm right-shift in the nucleobase spectra, the active pharmacophore fragment $[Et_3PAu]^+$ possesses a very characteristic UV–vis spectrum with a strong HOMO→LUMO band at

325.7 nm, whose disappearance may be a robust indication of its coordination (to the nucleobases) in *in vitro* assays.

We envision that the here presented computational results may lay an important cornerstone for future experimental and theoretical studies particularly focused on the interaction of AF and its analogues towards DNA and RNA.

CRediT authorship contribution statement

Iogann Tolbatov: Writing – review & editing, Writing – original draft, Data curation, Conceptualization. **Paolo Umari:** Writing – original draft, Conceptualization. **Tiziano Marzo:** Writing – original draft, Conceptualization. **Lorenzo Chiaverini:** Writing – original draft, Conceptualization. **Diego La Mendola:** Writing – original draft, Conceptualization. **Alessandro Marrone:** Writing – review & editing, Writing – original draft, Supervision, Data curation, Conceptualization.

Declaration of competing interest

The authors declare that they have no known competing financial interests or personal relationships that could have appeared to influence the work reported in this paper.

Data availability

Data will be made available on request.

Acknowledgements

This work has been funded by the European Union - Next-Generation EU ("PNRR M4C2-Investimento 1.4- CN00000041"). We acknowledge the CINECA award under the ISCRA initiative, for the availability of high performance computing resources and support. IT gratefully acknowledges the usage of HPC resources from Direction du Numérique – Centre de Calcul de l'Université de Bourgogne (DNUM CCUB), France. TM thanks the financial support from Ministero Italiano dell'Università e della Ricerca (MUR, Italy) under the program PRIN 2022—Progetti di Rilevante Interesse Nazionale, project code: 2022ALJRPL "Biocompatible nanostructures for the chemotherapy treatment of prostate cancer".

Appendix A. Supplementary data

Supplementary data to this article can be found online at https://doi.org/10.1016/j.cplett.2024.141197.

References

[1] V. Brabec, O. Hrabina, J. Kasparkova, Cytotoxic platinum coordination compounds. DNA binding agents, Coord. Chem. Rev. 351 (2017) 2–31.
[2] B.A. Carneiro, W.S. El-Deiry, Targeting apoptosis in cancer therapy, Nat. Rev. Clin. Oncol. 17 (7) (2020) 395–417.
[3] I. Tolbatov, A. Marrone, Reaction of dirhodium and diruthenium paddlewheel tetraacetate complexes with nucleophilic protein sites: a computational study, Inorg. Chim. Acta 530 (2022) 120684.
[4] L. Chen, G.A. Calin, S. Zhang, Novel insights of structure-based modeling for RNA-targeted drug discovery, J. Chem. Inf. Model. 52 (10) (2012) 2741–2753.
[5] A.E. Hargrove, Small molecule–RNA targeting: starting with the fundamentals, Chem. Commun. 56 (94) (2020) 14744–14756.
[6] M.J. O'Connor, Targeting the DNA damage response in cancer, Mol. Cell 60 (4) (2015) 547–560.
[7] S.T. Crooke, J.L. Witztum, C.F. Bennett, B.F. Baker, RNA-targeted therapeutics, Cell Metab. 27 (4) (2018) 714–739.
[8] M. Brunderová, M. Krömer, M. Vlková, M. Hocek, Chloroacetamide-modified nucleotide and RNA for bioconjugations and cross-linking with RNA-binding proteins, Angew. Chem. Int. Ed. 62 (7) (2022) e202213764.
[9] R. Taylor, P. Kotian, T. Warren, R. Panchal, S. Bavari, J. Julander, S. Dobo, A. Rose, Y. El-Kattan, B. Taubenheim, Y. Babu, BCX4430–a broad-spectrum antiviral adenosine nucleoside analog under development for the treatment of Ebola virus disease, J. Infect. Public Health 9 (3) (2016) 220–226.
[10] R.J. Geraghty, M.T. Aliota, L.F. Bonnac, Broad-spectrum antiviral strategies and nucleoside analogues, Viruses 13 (4) (2021) 667.
[11] J.M. Thomson, I.L. Lamont, Nucleoside analogues as antibacterial agents, Front. Microbiol. 10 (2019) 952.
[12] M. Guinan, C. Benckendorff, M. Smith, G.J. Miller, Recent advances in the chemical synthesis and evaluation of anticancer nucleoside analogues, Molecules 25 (9) (2020) 2050.
[13] M. Groessl, Y.O. Tsybin, C.G. Hartinger, B.K. Keppler, P.J. Dyson, Ruthenium versus platinum: interactions of anticancer metallodrugs with duplex oligonucleotides characterised by electrospray ionisation mass spectrometry, J. Biol. Inorg. Chem. 15 (2010) 677–688.
[14] E.R. Jamieson, S.J. Lippard, Structure, recognition, and processing of Cisplatin–DNA adducts, Chem. Rev. 99 (9) (1999) 2467–2498.
[15] K.J. Franz, N. Metzler-Nolte, Introduction: metals in medicine, Chem. Rev. 119 (2) (2019) 727–729.
[16] V.M. Miranda, Medicinal inorganic chemistry: an updated review on the status of metallodrugs and prominent metallodrug candidates, Rev. Inorg. Chem. 42 (1) (2022) 29–52.
[17] V. Graziani, A. Marrone, N. Re, C. Coletti, J.A. Platts, A. Casini, A multi-level theoretical study to disclose the binding mechanisms of gold (III)–bipyridyl compounds as selective aquaglyceroporin inhibitors, Chem. A Eur. J. 23 (55) (2017) 13802–13813.
[18] C. Gabbiani, A. Casini, L. Messori, Gold (III) compounds as anticancer drugs, Gold Bull. 40 (2007) 73–81.
[19] G. Gasser, I. Ott, N. Metzler-Nolte, Organometallic anticancer compounds, J. Med. Chem. 54 (1) (2011) 3–25.
[20] I. Tolbatov, A. Marrone, C. Coletti, N. Re, Computational studies of Au (I) and Au (III) anticancer metallodrugs: a survey, Molecules 26 (24) (2021) 7600.
[21] S. Scoditti, F. Chiodo, G. Mazzone, S. Richeter, E. Sicilia, Porphyrins and metalloporphyrins combined with N-heterocyclic carbene (NHC) gold (I) complexes for photodynamic therapy application: what is the weight of the heavy atom effect? Molecules 27 (13) (2022) 4046.
[22] H.F. Dos Santos, Reactivity of auranofin with S-, Se-and N-containing amino acids, Comput. Theor. Chem. 1048 (2014) 95–101.
[23] C. Roder, M.J. Thomson, Auranofin: repurposing an old drug for a golden new age, Drugs R&D 15 (2015) 13–20.
[24] D. Cirri, T. Marzo, I. Tolbatov, A. Marrone, F. Saladini, I. Vicenti, F. Dragoni, A. Boccuto, L. Messori, In vitro anti-SARS-CoV-2 activity of selected metal compounds and potential molecular basis for their actions based on computational study, Biomolecules 11 (12) (2021) 1858.
[25] T. Marzo, D. Cirri, C. Gabbiani, T. Gamberi, F. Magherini, A. Pratesi, A. Guerri, T. Biver, F. Binacchi, M. Stefanini, A. Arcangeli, Auranofin, Et_3PAuCl, and Et_3PAuI are highly cytotoxic on colorectal cancer cells: a chemical and biological study, ACS Med. Chem. Lett. 8 (10) (2017) 997–1001.
[26] S. Shen, J. Shen, Z. Luo, F. Wang, J. Min, Molecular mechanisms and clinical implications of the gold drug auranofin, Coord. Chem. Rev. 493 (2023) 215323.
[27] Zhang, Zhao, Y., Wang, X., Qi, C., Tian, J., Zou, Z., 2023. Synergistic lethality between auranofin-induced oxidative DNA damage and ATR inhibition in cancer cells. Life Sci. 332, pp. 122131.
[28] F.H. Abdalbari, C.M. Telleria, The gold complex auranofin: new perspectives for cancer therapy, Discover Oncol. 12 (2021) 42.
[29] Diaz, R. S., Shytaj, I. L., Giron, L. B., Obermaier, B., della Libera, E., Galinskas, J., Dias, D., Hunter, J., Janini, M., Gosuen, G., Ferreira, P- A., Sucupira, M. C., Maricato, J., Fackler, O., Lusic, M., Savarino, A., 2019. Potential impact of the antirheumatic agent auranofin on proviral HIV-1 DNA in individuals under intensified antiretroviral therapy: Results from a randomised clinical trial. Int. J. Antimicrobial Agents, 54(5), pp. 592-600.
[30] C.K. Mirabelli, C.-M. Sung, J.P. Zimmerman, D.T. Hill, S. Mong, S.T. Crooke, Interactions of gold coordination complexes with DNA, Biochem. Pharmacol. 35 (9) (1986) 1427–1433.
[31] J. Bondeson, R. Sundler, Auranofin inhibits the induction of interleukin 1β and tumor necrosis factor α mRNA in macrophages, Biochem. Pharmacol. 50 (11) (1995) 1753–1759.
[32] E. Isakov, P. Weisman-Shomer, M. Benhar, Suppression of the pro-inflammatory NLRP3/interleukin-1β pathway in macrophages by the thioredoxin reductase inhibitor auranofin, Biochim. Biophys. Acta (BBA) - General Subjects 1840 (10) (2014) 3153–3161.
[33] X. Luo, Y. Su, L. Zhong, Q. Kuang, Y. Zhu, X. Zhou, G. Tang, Y. Fu, S. Li, R. Wu, Auranofin ameliorates psoriasis-like dermatitis in an imiquimod-induced mouse by inhibiting of inflammation and upregulating FA2H expression, Biomed. Pharmacother. 160 (2023) 114421.
[34] M. J. Frisch, G. W. Trucks, H. B. Schlegel et al. Gaussian 16, Revision C.01, Gaussian, Inc., Wallingford CT, 2016.
[35] G. Sciortino, J.D. Maréchal, E. Garribba, Integrated experimental/computational approaches to characterize the systems formed by vanadium with proteins and enzymes, Inorg. Chem. Front. 8 (8) (2021) 1951–1974.
[36] T. Marino, N. Russo, M. Toscano, M. Pavelka, On the metal ion (Zn 2+, Cu 2+) coordination with beta-amyloid peptide: DFT computational study, Interdisciplinary Sci. Comput. Life Sci. 2 (2010) 57–69.
[37] I. Tolbatov, N. Re, C. Coletti, A. Marrone, An insight on the gold (I) affinity of golB protein via multilevel computational approaches, Inorg. Chem. 58 (16) (2019) 11091–11099.
[38] T. Marino, N. Russo, M. Toscano, M. Pavelka, Theoretical investigation on DNA/RNA base pairs mediated by copper, silver, and gold cations, Dalton Trans. 41 (6) (2012) 1816–1823.
[39] J.-D. Chai, M. Head-Gordon, Long-range corrected hybrid density functionals with damped atom-atom dispersion corrections, PCCP 10 (2008) 6615–6620.

[40] D. Andrae, U. Häußermann, M. Dolg, H. Stoll, H. Preuß, Energy-adjusted ab initio pseudopotentials for the second and third row transition elements, Theor. Chim. Acta 77 (1990) 123–141.
[41] F. Weigend, R. Ahlrichs, Balanced basis sets of split valence, triple zeta valence and quadruple zeta valence quality for H to Rn: design and assessment of accuracy, PCCP 7 (18) (2005) 3297–3305.
[42] I. Tolbatov, A. Marrone, Kinetics of reactions of dirhodium and diruthenium paddlewheel tetraacetate complexes with nucleophilic protein sites: computational insights, Inorg. Chem. 61 (41) (2022) 16421–16429.
[43] I. Tolbatov, A. Marrone, Reactivity of N-heterocyclic carbene half-sandwich Ru-, Os-, Rh-, and Ir-based complexes with cysteine and selenocysteine: a computational study, Inorg. Chem. 61 (1) (2021) 746–754.
[44] Tolbatov, I., Marrone, A., Paciotti, R., Re, N., Coletti, C., 2021. Multilayered modelling of the metallation of biological targets. In: Computational Science and Its Applications–ICCSA 2021: 21st International Conference, Cagliari, Italy, September 13–16, 2021, Proceedings, Part X 21 (pp. 398-412). Springer International Publishing.
[45] J. Tomasi, B. Mennucci, E. Cancès, The IEF version of the PCM solvation method: an overview of a new method addressed to study molecular solutes at the QM ab initio level, J. Mol. Struct. (Thoechem) 464 (1–3) (1999) 211–226.
[46] A.D. Becke, Density-functional exchange-energy approximation with correct asymptotic behavior, Phys. Rev. A 38 (6) (1988) 3098–3100.
[47] C. Lee, W. Yang, R.G. Parr, Development of the Colle-Salvetti correlation-energy formula into a functional of the electron density, Phys. Rev. B 37 (2) (1988) 785.
[48] E.D. Glendening, C.R. Landis, F. Weinhold, NBO 6.0: natural bond orbital analysis program, J. Comput. Chem. 34 (16) (2013) 1429–1437.
[49] P.F. Santiago, J.R.S. Mercado, B.M. Brito, DFT/TD-DFT studies on electronic and photophysical properties of Auranofin: a reference Au (I) complex, Polyhedron 180 (2020) 114262.
[50] X. Zhang, K. Selvaraju, A.A. Saei, P. D'Arcy, R.A. Zubarev, E.S. Arnér, S. Linder, Repurposing of auranofin: thioredoxin reductase remains a primary target of the drug, Biochimie 162 (2019) 46–54.